The Activation and Inhibition of Cyclin-Dependent Kinase-5 by Phosphorylation†

B. Zhang,‡,§ V. B. C. Tan,*,§ K. M. Lim,§ and T. E. Tay§

Department of Chemistry, Zhejiang University, Hangzhou 310027, P. R. China, and Department of Mechanical Engineering, National University of Singapore, S117576, Singapore

Received May 11, 2007; Revised Manuscript Received June 26, 2007

ABSTRACT: Despite the very similar 3-dimensional structures as reflected by the more than 60% identity in amino acid sequences, CDK2 and CDK5 have very different functions and characteristics. Phosphorylation on a conserved Thr14 can inhibit activities of both the kinases, but phosphorylating another conserved Tyr15, however, can lead to totally opposite inhibition and stimulation consequences in CDK2 and CDK5. Our molecular dynamics (MD) simulations suggest a similar inhibition mechanism of phosphorylation on the Thr14 as in the CDK2 system. In both the systems, the kinase activities are inhibited by the phosphorylation because it causes ATP phosphate moiety misalignment and changes in the Mg^{2+} ion coordination sphere, which have been proven to be critical for the phosphate group of the ATP transferring to the hydroxyl group on the serine in the substrate peptide. The calculations indicate that ATP adopts a more favorable conformation and location in the phosphorylated Tyr15 complex to facilitate the interactions with the substrate and the Mg^{2+} is wrapped more strongly by the phosphate group than in the unphosphorylated system, which might be favored by the transfer reaction.

Cyclin-dependent kinase 5 (CDK5), also known as neuronal CDK2-like kinase, is a unique member of the small serine/threonine CDK[1] family, in which most of the family members play a central role in the control of the eukaryotic cell division cycle (*1*−*3*). CDK5 was discovered in the early 1990s (*4*), and since then, great progress has been made in identifying this multifunctional kinase. The best known role for CDK5 is in regulating the cytoarchitecture of the central nervous system (CNS), but there is also evidence that links CDK5 activity to the regulation of the cytoskeleton, axon guidance, membrane transport, synaptic function, dopamine signaling, and drug addiction (*4*, *5*). Recent investigations have revealed that CDK5 is involved in biological pathways important for several diseases, such as Alzheimer's disease, amyotropic lateral sclerosis (ALS), Parkinson's disease, etc. (*6*−*10*).

Structures of CDK5 determined to date by X-ray diffraction studies show that, as with other CDKs (*11*−*15*), CDK5 possesses a fold comprising an N-terminal domain composed largely of a β-sheet with one helix, the C helix (residues PSAALRE), whose correct orientation is important for catalysis, and a larger C-terminal domain composed of mostly α-helices. Close to the C helix is an inhibitory loop, the glycine-rich loop (G-loop), whose primary sequence includes three highly conserved glycine residues. The G-loop plays an important role in the CDK activity regulation and forms the "ceiling" of the ATP-binding site, which is also called the catalytic site. The site is at the domain interface with residues important for ATP binding contributed from both domains and residues important for substrate peptide binding located almost exclusively in the C-terminal domain. These eukaryotic protein kinases catalyze the phosphoryl transfer of the γ-phosphate group of ATP to the serine, threonine, or tyrosine residue of protein substrates, which include the neuron-specific cytoskeletal proteins Neurofilament and Tau, the L1S1 and Dynein-associated protein Nudel, etc. (*16*−*24*). Phosphorylation of the target protein can have dramatic downstream consequences, leading to conformational response, activation or inhibition of catalytic activity, association or dissociation of complexes, and translocation to different cell compartments (*25*).

As with other CDKs, active CDK5 is also a proline-directed kinase that phosphorylates in vitro serines and threonines immediately upstream of a proline residue (*5*). In addition to an absolute requirement for proline in the +1 postion (*26*, *27*), CDK5 shows a marked preference for a basic residue in the +3 position and phosphorylates the consensus sequence (S/T)PX(K/H/R), where S or T is the phosphorylatable serine or threonine, X is any amino acid, and P is the proline residue in the +1 position. In this family, both CDK1 and CDK2 have an identical substrate specificity to that described for CDK5 (*28*). Like other CDKs, monomeric CDK5 shows no enzymatic activity and requires association with a regulatory partner for activation (*5*).

Normally, activities of CDKs are regulated by multiple mechanisms that include inhibitory or activated phosphorylation of conserved residues in the inhibition loop (G-loop) and/or activation loop (T-loop) (*29*−*30*). The G-loop has two possible phosphorylation sites, Thr14 and Tyr15. Phosphorylation of both the residues by the dual specificity kinase

* Corresponding author. Tel: 65-6516 8808. Fax: 65-6779 1459. E-mail: mpetanbc@nus.edu.sg.

‡ Zhejiang University.

§ National University of Singapore.

† This work was supported by the Ministry of Education, Singapore (Grant R265000245112).

[1] Abbreviations: CDK, cyclin-dependent kinase; MD, molecular dynamics; G-loop, glycine-rich loop; T-loop, activation loop; HB, hydrogen bonding; pT14/CDK5/p25/ATP/HHASPRK or pT14, phosphorylated-Thr14/CDK5/p25/ATP/HHASPRK; pY15/CDK5/p25/ATP/HHASPRK or pY15, phosphorylated-Tyr15/CDK5/p25/ATP/HHASPRK.

10.1021/bi700890t CCC: $37.00
Published on Web 08/22/2007

Wee1 and Myt1 normally inhibits CDK activity, whereas phosphorylation of Thr160 in the T-loop of CDK2 (or Thr161 of CDK1) by the CDK-activiated kinase (CAK) is necessary for maximal activation (*31*). However, in spite of the very similar 3-dimensional structures as reflected in their sequence identity of 60% between CDK2 and CDK5, the latter has different regulation mechanisms. Although Tyr15 is well conserved in CDK5, it cannot be phosphorylated by Weel1 in vitro (*32*); instead, it is phosphorylated by c-Abl, and this phosphorylation is enhanced by association of CDK5 with an Abl-binding adaptor protein called Cables (*33*). Unexpectedly, phosphorylation of CDK5 on Tyr15 is stimulatory and increases CDK5 kinase activity, which is totally contrary to what happens in CDK1 and CDK2.

Recently, the crystal structure of phosphor-CDK2/cyclinA in complex with Mg^{2+} ADP, nitrate, and a heptapeptide substrate was determined to study the catalytic mechanism by using both structural and kinetic studies (*34*). The results support the notion that the protein kinase reaction proceeds through a mostly dissociative mechanism with a trigonal planar metaphosphate intermediate. Bártová et al. (*35*, *36*) and Endicott et al. (*37*) explained the mechanisms of inhibition of phosphorylation of Thr14 and Tyr15, theoretically and experimentally, respectively. It was proposed that inhibitory phosphorylation of Thr14 causes ATP misalignment and a shift of the magnesium ion. This leads to an increase in the Ser−ATP distance (*35*, *36*). According to Endicott et al. (*37*), the mechanism of inhibition phosphorylation on the Tyr15 is quite different from that of the Thr14. Their crystal structure shows that the phosphorylated Tyr15 side chain adopts a "swung out" conformation so that the phosphate group is exposed to the solvent and sterically blocks the binding of the peptide substrate and consequently reduces the CDK2/substrate binding affinity.

The objective of this work is to study the dynamics of the unphosphorylated CDK5/p25/ATP/HHASPRK, phosphorylated-Thr14/CDK5/p25/ATP/HHASPRK (pT14/CDK5/p25/ATP/HHASPRK or pT14), phosphorylated-Tyr15/CDK5/p25/ATP/HHASPRK (pY15/CDK5/p25/ATP/HHASPRK or pY15), in particular, the interactions of CDK5 with ATP and with peptide substrate. Findings from our simulations will be compared with the behaviors of the CDK2 systems inhibited by phosphorylation in the inhibitory sites Thr14 and Tyr15 to shed light on the different inhibition/activation mechanisms in CDK2 and CDK5 systems.

It is worthy of note that there are different conformations of the unphosphorylated Tyr15 side chain in some CDK2 crystal structures (*34*, *37*, *38*), and the "swung out" phosphorylated Tyr15 can give strong evidence of the inhibition mechanism for CDK2. Considering the similarities between 3D structures of CDK2 and CDK5, if the phosphorylated Tyr15 in CDK5 also adopts a flipped-out conformation like that in the CDK2 complex, one might also imagine a similar interaction mode between the phosphate group on the residue and the substrate peptide, which might imply a similar inhibitory mechanism. However, as mentioned previously, Tyr15 in CDK5 cannot be phosphorylated by the protein Wee1 (*32*), which normally phosphorylates Tyr15 in CDK2. Instead, it is phosphorylated by c-Abl. Thus, it can be speculated that conformations of Tyr15 can be adjusted when it is being phosphorylated because of the different interactions between phosphorylation proteins and the CDKs. In the present work, phosphate groups are simply added onto the original Thr14 and Tyr15 to present the phosphorylations due to lack of experimental data showing any possibility of the change of the Tyr15 before or after phosphorylation.

MATERIALS AND METHODS

Molecular Dynamics Simulations. Molecular dynamics simulations were carried out using the SANDER module of AMBER 8.0 with the Cornell et al. all-atom force field (*39*). Prior to the MD simulations, the values for some of the force field parameters for the ligands had to be developed because of the lack of reported data. Optimization of the ligands was first achieved with the Gassuian98 package at the HF/6-31G* theoretical level. Electrostatic potentials (ESP) were then generated with Merz−Singh−Kollman van der Waals parameters (*40*). Fitting of the charges to the ESP was performed with the RESP program (*41*) of the AMBER package. GAFF (*42*) force field parameters and RESP partial charges were assigned using the ANTECHAMBER module.

The starting geometries for the simulations of all the complexes were generated from X-ray structures obtained from the Protein Data Bank (PDB ID code: 1UNL, 1QMZ, respectively). Phosphorylations of the Thr14 and the Tyr15 were derived from manual modifications of the crystal structure of CDK5/p25/roscovitine (1UNL). ATP and HHASPRK are generated from the crystal structure of CDK2/cyclinA/ATP/HHASPRK.

All simulations are at neutral pH. Lys and Arg residues are positively charged, and Asp and Glu residues are negatively charged. The default His protonation state in Amber8 is adopted. Counterions were added to maintain the eletroneutrality of all the systems. Each system was immersed in a 10 Å layer truncated octahedron periodic water box. The layer of water molecule in all cases contained around 11,000 TIP3P (*43*) water molecules in each of the complexes. A 2 fs time step was used in all the simulations, and long-range electrostatic interactions were treated with the particle mesh Ewald (PME) procedure (*44*) using a cubic B-spline interpolation and a 10^{-5} tolerance for the direct-space and with a 12 Å nonbonded cutoff. Bond lengths involving hydrogen atoms were constrained using the SHAKE algorithm (*45*). All systems were minimized prior to the production run. The minimization, performed with the SANDER module under constant volume condition, consists of 4 steps. All heavy atoms in both proteins and ligands were restrained with degressive forces of 500, 100, 5 kcal/mol, respectively. In the first 3 steps, minimization of the solvent molecules and hydrogen atoms of the systems involved 250 cycles of steepest descent followed by 250 cycles of conjugate gradient minimization. All systems were then relaxed by 500 cycles of steepest descent and 1000 cycles of conjugate gradient minimization in the last step. Then, after a 2 ps molecular dynamics relaxation under NPT conditions, the whole system was heated to 300 K in steps. The system was first heated to 100 K during 10 ps and then to 200 K during the next 10 ps, and then to 250 K in another 10 ps. Finally, it was heated to 300 K in the last 20 ps. The production parts of all the systems took 5 ns in the NPT ensemble at 300 K with Berendsen (*46*) temperature coupling and constant pressure (1 atm) with isotropic molecule-based scaling (*46*).

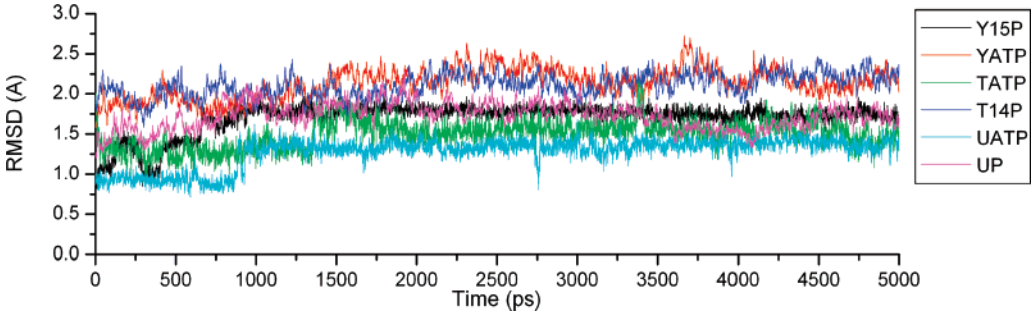

FIGURE 1: The root-mean-square deviations from starting structures for CDK5/p25 and ATP in the unphosphorylated (UP, UATP), the pT14 (T14P, TATP) and the pY15 (Y15P, YATP) complexes.

MM-PBSA Calculations. Binding free energies and energy decomposition of all the systems were analyzed using the MM-PBSA (molecular mechanics Poisson−Boltzmann/surface area) (*47*) approach to highlight the electrostatic and van der Waals contributions in the binding of ATP, substrate and ion with the kinase.

The binding free energies(ΔG_{bind}) were computed as

$$\Delta G_{bind} = \Delta G(\text{complex}) - [\Delta G(\text{protein}) + \Delta G(\text{ligand})] \quad (1)$$

$$\Delta G_{bind} = \Delta E_{gas} + \Delta\Delta G_{solv} - T\Delta S \quad (2)$$

$$\Delta E_{gas} = \Delta E_{int} + \Delta E_{ele} + \Delta E_{vdw} \quad (3)$$

$$\Delta G_{solv} = \Delta G_{PB} + \Delta G_{nonpolar} \quad (4)$$

The sum of molecular mechanical energies, ΔE_{gas}, can be divided into contributions from internal energy (ΔE_{int}), electrostatic potential (ΔE_{ele}), and van der Waals (ΔE_{vdw}) potential. The solvation free energy (ΔG_{solv}) is composed of two parts: polar solvation free energy (ΔG_{PB}) and nonpolar salvation free energy ($\Delta G_{nonpolar}$). All energies are averaged along the MD trajectories. The snapshots of each system were sampled from the last 3 ns single trajectory with an interval of 20 ps. The single trajectory approach is applied to estimate the energies. Estimation of energies in this manner has proven successful in our previous (*48*, *49*) and many other studies (*50*−*52*). Part of the reason for the success of this approach is the cancellation of errors that hides the effect of incomplete sampling. A better approach may be the use of separate trajectories of protein−ligand complex, free protein, and free ligand. Unfortunately, due to sampling limitations, the separate trajectory approach appeared to be significantly less stable. E_{gas} was obtained using SANDER, and estimation of ΔG_{PB} was conducted with a built-in module, PBSA in AMBER. $G_{nopolar}$ was determined from eq 5,

$$\Delta G_{nopolar} = \gamma A + b \quad (5)$$

where A is the solvent-accessible surface area estimated using Sanner's algorithm (*53*) with a solvent probe radius of 1.4 Å and the PARSE atomic radii parameters (*54*). γ and b are empirical constants and are set to 0.00542 and 0.92 kcal/mol, respectively.

RESULTS

Compared with the initial structures, no major structural changes are found in the kinases during all the simulations, except for some minor ones in the inhibition loop (G-loop) of the p15Y/CDK5/p25/ATP/HHASPRK. However, obvious conformational changes or displacement of ATP are observed during the first 1.5 ns of the three simulations compared with the conformation in the crystal structures as indicated by deviations in the root-mean-square from both the initial structure (Figure 1) and the time-averaged structures over our 5 ns simulations (Figure 2).

Important dihedral angles and distances in the averaged and the initial structures are listed in Table 1 to show the ATP conformational changes, the displacement of the ATP phosphate group, and the coordination bonding network around the Mg^{2+} ion during the simulations (see Scheme 1 for atom labeling). The dihedral angle between the adenine and ribose moieties, $C^6-N^1-C^5-C^4$, is used to depict the whole conformation change by revealing the relative positions of the long phosphate group and the adenine part. The other dihedral angles are employed to describe the conformation of the ATP phosphate group. The distances between the phosphorus atoms indicate the displacement of the ATP phosphate group during the simulations. $\gamma P-O^{ser}$ denotes the distance between the terminal phosphorus on the ATP phosphate group and the hydroxyl oxygen atom on the serine of the peptide substrate. All the distances involving Mg^{2+} are used to define the coordination environment around the ion.

Inhibition Mechanism of Phosphorylation on the Thr14. Dramatic conformational changes and reorientation of ATP occurred in the pT14 complex within the pT14/CDK5/p25/ATP/HHASPRK. From Table 1, it can be seen that distances between the αP, βP, and γP of the ATP in the initial and averaged structures are 3.49 Å, 5.03 Å, and 4.14 Å, respectively, implying an obvious shift of the phosphate group toward the margin of the ATP-binding cleft. The reorientation of the phosphate group also results in a 2.78 Å shift ($Mg^{2+}{}_I-Mg^{2+}{}_A$) of the Mg^{2+} ion position. The rotations of torsion angles $C^2-C^1-O^{10}-\alpha P$ and $\beta P-O^6-\gamma P-O^3$ make O^7 and O^8 on the αP and O^2 and O^3 on the γP approach the relocated Mg^{2+} to establish a stronger four-oxygen coordinated network instead of the three-oxygen (O^2, O^8, and O^6) coordination sphere in the initial structure. The displacement of the phosphate group causes a loss of O^{D1} coordination by Asn144 (distance between the ion and the O^{D1} increases from 1.85 Å to 4.97 Å), and no other contributors, such as water molecules or residues, are detected around the ion to offer the sixth coordination interaction.

Structural Analyses of p15Y/CDK5/p25/ATP/HHASPRK and CDK5/p25/ATP/HHASPRK Systems. A periodical movement of G-loop is detected in our simulations, but only in the unphosphorylated complex. No conformational change of the G-loop has been reflected during the p14T/CDK5/

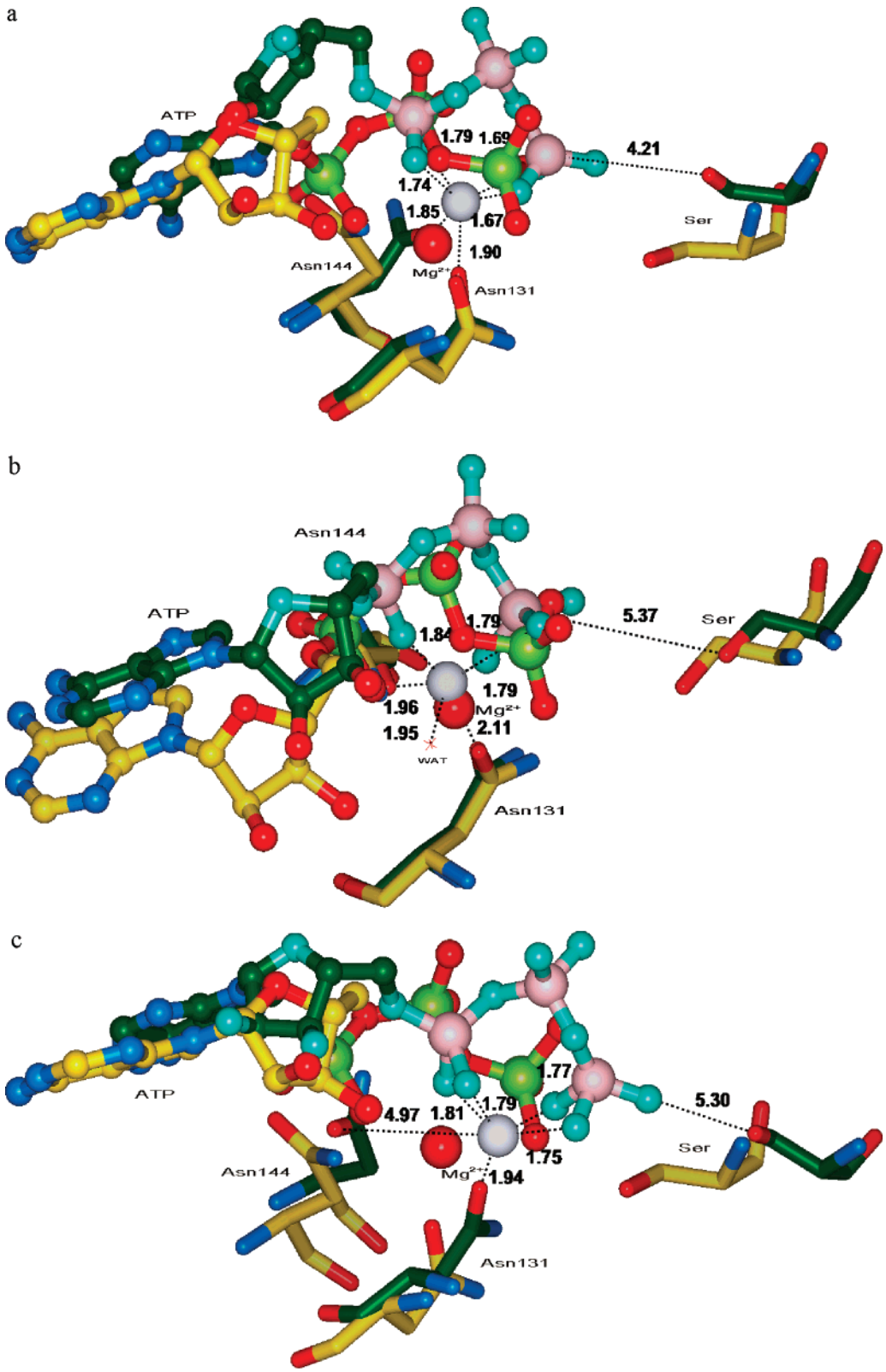

FIGURE 2: Superimposed initial and averaged structures of ATP and coordination sphere of Mg^{2+} in the pY15 (a), the unphosphorylated (b), and the pT14 systems (c). All the hydrogen atoms are omitted for clarity. All the oxygen atoms in the averaged and initial structure of ATP are colored light blue and red, respectively; phosphorus, pink and light green, respectively; carbon, dark green and yellow, respectively; ion, light gray and red, respectively.

p25/ATP/HHASPRK simulations. In contrast to the pT14 complex, both the Thr14 and the pY15 present a much more stretched conformation in the pY15/CDK5/p25/ATP/HHASPRK system, and the G-loop moves away from the PSAALRE direction as shown in Figure 3a. In comparing the positions of the pT15 and the Thr14 in the averaged structure with those in the initial structure, it is measured that the hydroxybenzene group moves (outward and downward) by 4.03 Å with the C^B atom of the Thr14, 6.72 Å moving along the same direction as the pY15, as shown in

Table 1: Geometrical Parameters in All the Complexes

	initial structure	pY15	unphosphorylated	pT14
$C^2-C^1-O^{10}-\alpha P$[a]	−137.4	−170.4	−173.2	−147.1
$\beta P-O^6-\gamma P-O^3$	46.9	130.8	141.4	124.8
$C^1-O^{10}-\alpha P-O^8$	65.8	156.4	−128.6	75.1
$\gamma P-O^9-\beta P-O^4$	−99.4	−179.8	−109.7	−66.3
$O^9-\beta P-O^6-\gamma P$	159.3	116.2	69	56.6
$C^6-N^1-C^5-C^4$	−59	−72.4	−92.2	−103.9
$\alpha P-\alpha P$[b]		1.27	1.50	3.49
$\beta P-\beta P$		2.51	1.35	5.03
$\gamma P-\gamma P$		2.82	1.78	4.14
$Mg^{2+}{}_I-Mg^{2+}{}_A$[c]		1.49	0.75	2.78
$Mg^{2+}-O^2$	2.25	1.67	1.79	1.75
$Mg^{2+}-O^3$		1.69	1.79	1.77
$Mg^{2+}-O^6$	2.12			
$Mg^{2+}-O^7$		1.79		1.81
$Mg^{2+}-O^8$	2.07	1.74	1.84	1.79
$Mg^{2+}-O^{Asn131}$	1.25	1.90	2.12	1.94
$Mg^{2+}-O^{Asn144}$		1.85	1.96	4.97
$Mg^{2+}-N^{Asn144}$	1.85			
$Mg^{2+}-O^{WAT}$			1.95	
$\gamma P-O^{ser}$	3.68	4.21	5.37	5.30

[a] Unit: degree (°). [b] Unit: angstrom (Å). [c] I = initial structure, A = averaged structure.

Scheme 1: Structure of ATP with Atom Labeling Used in This Article

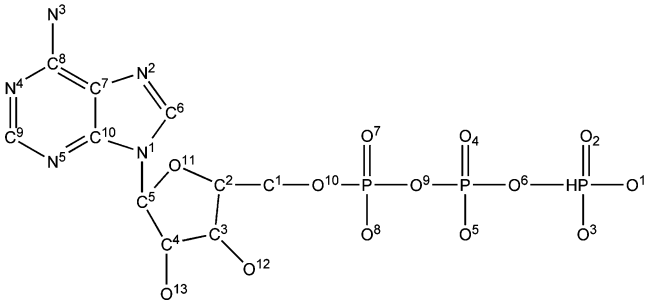

Figure 3a. However, the movements of the residues are terminated when strong hydrogen bonds (HB) are formed between the pY15 phosphate group and the N^Z of the Lys33 (Table 2), similar to what happens between the O^{3P} on the pT14 and the N^Z on the Lys33 in the pT14 complex. From Table 2, it can be seen that strong HBs are established between the O^4, O^5 on the βP in the ATP phosphate group and the N or O^{G1} on the Thr14 almost throughout the whole simulation. Thus, together with the displacement of the Thr14, the βP is also pulled 2.51 Å away from the original position in the pY15 complex. Consequently, the dramatic movement of the βP affects the conformation of the rest of the phosphate group. By looking at the variations of the values of the torsion angles $\beta P-O^6-\gamma P-O^3$ and $C^1-O^{10}-\alpha P-O^8$, from −99.4° to −179.8°, and from 65.8° to 156.4°, respectively, it is clear that both the αP and the γP moieties rotated to the new conformations. As a result, the O^2, O^3 on the γP and the O^7, O^8 on the αP move close enough to strongly coordinate with Mg^{2+}. Together with the coordination contributions from the Asn131 and Asn144, the Mg^{2+} eventually achieves a stable hexacoordinated sphere. Also, due to the rotation of the γP moiety, the O^1 on the γP points directly to the substrate serine, and form a very strong HB (the bond length is only 2.60 Å) with the hydroxyl group. In comparison with the distance of 5.37 Å for $\gamma P-O^{ser}$ in the CDK5/p25/ATP/ HHASPRK system, the $\gamma P-O^{ser}$ distance is only 4.21 Å in the p15Y/CDK5/p25/ATP/HHASPRK complex.

Our 5 ns simulations of the CDK5/p25/ATP/HHASPRK system also detected a 1.5 ns time scale periodical motion of the G-loop. However, the movement of the loop is not very obvious, and the RMSD value of the loop during the whole simulation time fluctuates between 0.5 Å and 1.4 Å, as shown in Figure 4. In Figure 3b, it is clear that the averaged G-loop only shifts slightly from the original position due to a small shift of the Thr14. The small shift of the Thr14 makes the apex of the loop move up slightly in comparison to the initial structure. Similar to what happens in the pY15 complex in the unphosphorylated combination, the O^{G1} and N in the Thr14 form strong HBs with the O^4 and O^5 on the βP, and the strong HBs lead to a rotation of the torsion angle $\beta P-O6-\gamma P-O3$ as well. This changes the conformation of the γP moiety. As a result, the γP moiety adopts a similar conformation to that in the pY15 combination. So the O^2 and O^3 on the γP can also coordinate with the Mg^{2+}. However, the slight movement of the Thr14 cannot influence the conformation of the αP moiety very significantly. The O^7 atom, therefore, cannot be rotated to the position as that in the pY15 complex to coordinate with the ion. Instead, a water molecule is detected around the ion to contribute the sixth coordination site. A 5 ns residence time of the water was traced during the simulation, and the averaged distance between the water molecule and Mg^{2+} is only 1.95 Å, indicating that the coordination of water is strong and stable.

Energetic Properties of All the Complexes. Considering the impracticality of normal mode calculations for the large size of these complexes and the uncertainties in the entropic calculation, entropic effects of the solute are not explicitly taken into account. For a series of compounds with similar structures and binding modes, the entropy contribution can be omitted if one is only interested in the relative order of binding affinities (*55*). Detailed information of the forces involved in ATP binding can be obtained by analyzing the MM-PBSA energy contributions, which are listed in Table 3 for all the systems. The total electrostatic interactions (ELE_{tot}) in the pY15, the pT14, and the unphosphorylated systems, which are composed of the gas phase (ELE_g) and the solvation electrostatic (ELE_s) contributions, are −181.57,

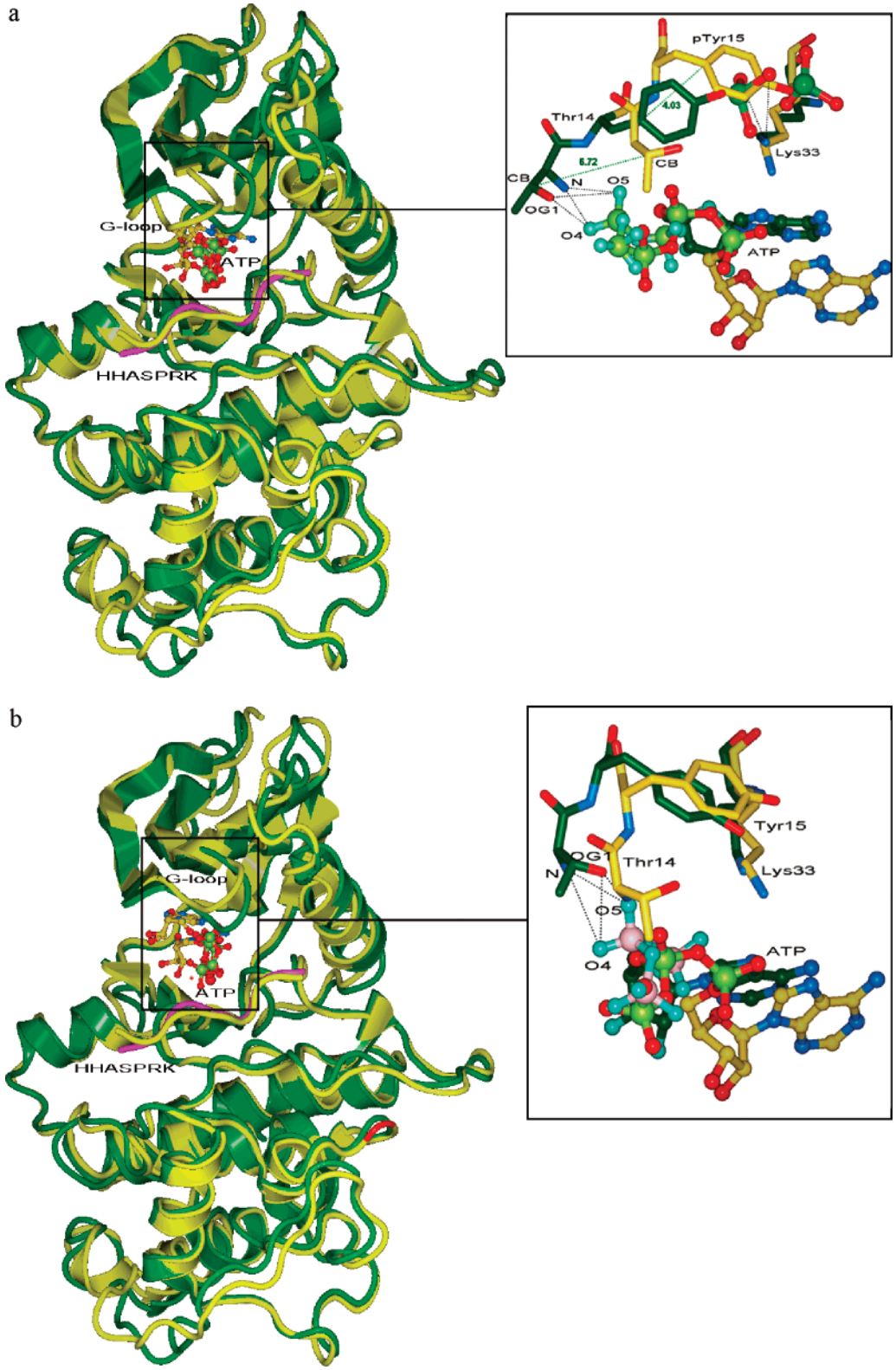

FIGURE 3: Superimposed initial (green) and averaged (yellow) structures of the pY15 (a) and the unphosphorylated (b) systems. CDK5 and the substrate peptide are schemed with solid ribbon. Conformations of Thr14, Tyr15, and Lys33 are presented by stick, and ATP, ball and stick.

−102.10, and −72.24 kcal/mol, respectively. The electrostatic contributions to the solvation energy of the pY15 and the unphsophorylated complexes are close to each other (1213.12 and 1280.74 kcal/mol, respectively), and both are higher than that of the pT14 combination.

To understand the importance of the water molecule in the CDK5/p25/HHASPRK system and the individual coordination contribution from each factor in the coordination sphere in both the p15Y and the unphosphorylated complexes, binding energies between the ion and the rest of the complex are calculated separately by including and excluding the water molecules. As given in Table 3, it is clear that the ELE_s (665 kcal/mol and 678 kcal/mol, respectively) and the VDW/nonpolar (34.84 kcal/mol and 30.22 kcal/mol, respec-

Table 2: Properties of Hydrogen Bonds in All the Complexes

complex	hydrogen bond	duration	mean distance (Å)	mean angle (deg)
pY15	O^4(ATP)···HN(Thr14)	95.97	2.90	23.16
	O^4(ATP)···HO^{G1}(Thr14)	91.66	2.73	18.02
	O^5(ATP)···HN(Gly16)	85.24	3.02	18.31
	N^3(ATP)···HN(Asn144)	74.37	3.05	28.06
	O^1(ATP)···HO^G(Ser)	72.25	2.60	13.72
	O^5(ATP)···HN (Thr14)	44.42	2.94	43.49
	O^5(ATP)···HO^{G1} (Thr14)	18.25	3.08	38.19
	O^3P(pY15)···$H^{Z1}N^Z$(Lys33)	34.20	2.84	23.24
	O^3P(pY15)···$H^{Z3}N^Z$(Lys33)	21.69	2.88	29.00
	O^3P(pY15)···$H^{Z3}N^Z$(Lys33)	18.93	2.86	25.40
	OE2(Glu51)···HN^3(ATP)	56.17	2.97	28.32
unphosphorylated	N^4(ATP)···HN(Cys83)	97.97	3.07	16.48
	O^5(ATP)···HO^G1(Thr14)	88.54	2.72	17.22
	O^5(ATP)···HN (Thr14)	86.93	2.82	25.28
	O^4(ATP)···HO^G1(Thr14)	16.84	2.86	17.40
	O^4(ATP)···HN (Thr14)	37.56	3.05	30.24
	O(Glu81)···HN^3(ATP)	99.18	2.96	23.02
	O(WAT6959)···HO^{13}(ATP)	81.32	2.70	14.92
pT14	O^2P(pT14)···$H^{Z1}N^Z$(Lys33)	91.22	2.80	20.87
	O^2P(pT14)···NH(Gly146)	92.21	2.98	29.28
	N^3(ATP)···$H^{Z2}N^Z$(Lys33)	64.46	2.89	22.57
	O^1P(pT14)···$H^{Z1}N^Z$(Lys33)	15.63	3.32	47.08
	O(WAT18742)···HO^{13}(ATP)	63.23	2.72	14.93
	N^{D2}(Asn144)···HN^3(ATP)	59.52	3.15	21.49
	O(WAT1577)···HN^3(ATP)	55.60	3.06	35.82

tively) contributions are similar when the water molecule is included or excluded; therefore, it seems the biggest difference of the binding affinities is mainly from the difference of the ELE_g contributions. In the CDK5/p25/ATP/HHASPRK complex, it can be seen that, with and without the coordination from the water molecule, the binding energies (*E*) are −341.62 kcal/mol and −262.42 kcal/mol, respectively, indicating a contribution of about −80 kcal/mol from the water molecule. Meanwhile, it is noticed that the ELE_g contributions, when the water molecule is included and excluded, are −1041.62 kcal/mol and −971.09 kcal/mol, respectively, which means around −70 kcal/mol energy difference out of the −80 kcal/mol contributes from the gas phase electrostatic interactions.

When combined with geometrical parameters in Table 1, the ELE_g and *E* coordination interactions from the O^8 (about −181 kcal/mol and −40 kcal/mol, respectively) can be calculated easily by comparing the electrostatic contribution and the binding energy in the pY15 with that in the water-excluded CDK5/p25/ATP/HHASPRK system. If we assume that these are averaged ELE_g and *E* contributions from the oxygen atoms on the ATP phosphate group, the total ELE_g and *E* contributions from the two residues, about −428 kcal/mol, −231 kcal/mol, respectively, thus, can be determined. That means the averaged ELE_g and *E* contributions from the residue are around −214 kcal/mol and −165 kcal/mol. Accordingly, the ELE_g and *E* contributions (−724 kcal/mol and −160 kcal/mol) from the four oxygen atoms on the phosphate group, which are around 63% and 45% out of the total ELE_g and *E* (−1194 kcal/mol and −352 kcal/mol) from all the coordination interactions, indicate a very strong chelation.

Binding of Substrate Peptide. The HHASPRK peptides are tightly bound to the substrate binding box throughout all the simulations. However, obvious and periodical oscillation of the RMSD curves of the peptides is detected during the simulations, as shown in Figure 5. To look into the interactions and dynamic properties of the peptide during the simulations, distances between the R side chain and the G-loop are traced to monitor the movement of the side chain in the CDK5 complexes. Our simulations suggest that the long side chain does not simply approach the negatively charged groups; instead, it keeps swinging during the simulations (Figure 5).

DISCUSSION

Inhibition Mechanism of Phosphorylation on the Thr14. Simulations from Bártová and his co-workers (*35*, *36*) suggested that the CDK2/cyclinA/ATP/HHASPRK system is inhibited by phosphorylation on the Thr14 because the phosphorylation causes ATP phosphate moiety misalignment and changes in the Mg^{2+} ion coordination sphere. It also causes the G-loop to shift away from the ATP binding site. Our calculations propose a similar inhibitory mechanism of phosphorylation on the G-loop Thr14 of CDK5. Considering the short distance (1.81 Å) between two big negatively charged phosphates groups on the phosphorylated Thr14 and ATP, respectively and possibly due to both the strong electrostatic repulsion and steric clashes between them in the initial structure, the occurrence of the dramatic conformational changes and reorientation of ATP in the pT14 complex during the simulations is understandable and reasonable. Except for the loss of the coordination by the Asn144, no water molecules are discovered around the ion to offer the sixth coordination interaction. It is possible that the rotation of the O^7 repels water molecules which originally can coordinate with the Mg^{2+} as shown in the crystal structure. All the analyses imply that the correct hexacoor-

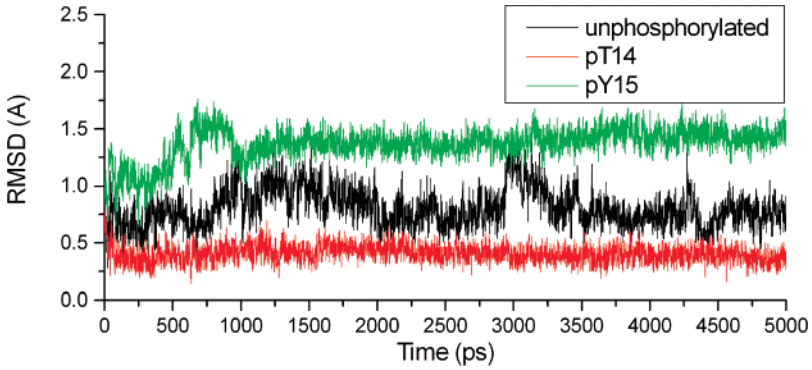

FIGURE 4: RMSD of G-loop in all systems.

Table 3: Energy Contributions of ATP, Mg^{2+} Binding with the Receptors[a]

ATP Binding			
	pY15	unphosphorylated	pT14
ELE_g	−1394.69	−1352.98	−1232.84
VDW	−8.09	−12.73	−6.94
$ELE_{nonpolar}$	−4.33	−4.39	−4.12
ELE_s	1213.12	1280.74	1130.73
E	−193.99	−89.36	−113.17

Mg^{2+} Binding				
		unphosphorylated		
	pY15	water included	water excluded	pT14
ELE_g	−1152.08	−1041.62	−971.09	−1194.78
VDW	40.29	35.37	30.64	39.30
$ELE_{nonpolar}$	−0.42	−0.43	−0.42	−0.42
ELE_s	720.93	665.05	678.45	803.34
E	−391.29	−341.62	−262.42	−352.56

[a] ELE_g: gas phase electrostatic interaction. VDW: gas phase van der Waals interaction. $ELE_{nonpolar}$: nonpolar contribution to the solvation energy. ELE_s: electrostatic contribution to the solvation energy. Unit: kcal/mol.

dination of the Mg^{2+} ion observed by a structural study has been changed. It has been suggested that the proper coordination, together with the appropriate orientation and conformation of ATP phosphate group, is crucial for the phosphate transfer reaction between ATP and the serine hydroxyl on the substrate (*34*−*36*). As a result, the loss of the kinase activity after the Thr14 phosphorylation in the CDK5 system can be explained similarly as that with the CDK2 complex.

Structural Analyses of p15Y/CDK5/p25/ATP/HHASPRK and CDK5/p25/ATP/HHASPRK Systems. The glycine-rich loop (G-loop) enables CDKs to adopt a wide range of backbone conformations. The significance and functional importance of this domain in cAMP-dependent protein kinases have been described in detail (*25*, *35*, *36*, *56*−*58*). Our results show that, although the pT14 group pushes the ATP phosphate group to a new position in the active site in the p14T/CDK5/p25/ATP/HHASPRK complex, no obvious influence has been found in the group itself and the conformation of the G-loop. This is probably because the strong HB interaction between the O^{3P} on the pT14 and the N^Z on the Lys33 (Table 2) anchors the phosphorylated threonine to its original position. The G-loop in the pY15 system has an obvious change compared to the pT14 complex (Figure 3a). This is illustrated by investigating the interactions from the environment around the pY15. The big phosphate group on the pY15 points into a relatively small cavity enclosed by two β-sheets (residues 66−71 and 75−81, respectively) and the PSAALRE α-helix in the initial structure. Thus, it is likely that strong electrostatic and steric interactions emerge between the pY15 and the small cavity. Consequently, the pY15 might be pushed out of the cavity. The movement of the pY15 and the Thr14 during the simulations affects not only the conformation of the G-loop but also the conformation of the ATP phosphate group and the coordination of the ion in the pY15 complex, and eventually leads to a more stable hexacoordinated sphere of the Mg^{2+}, which is, as mentioned above, crucial for the phosphate transfer to the substrate serine. It is worthy of note that the displacement of the Thr14 and the shift of the ATP phosphate group might be larger if not for the fixation of the pY15 by the Lys33 in the pY15 system. Consequently, the coordination network may not be organized correctly. Also, because of the conformational change of the γP moiety, the $\gamma P-O^{ser}$ in the pY15 complex is largely shortened compared to that in the unphosphorylated system, and a very strong HB with the serine hydroxyl group is established. Both the $\gamma P-O^{ser}$ distances in the two complexes are within the reasonable phosphate transfer reaction range (5.7 Å) (*34*). The significant decrease in the distance will undoubtedly facilitate the occurrence of the transfer reaction.

For the unphosphorylated complex, the phosphate group also adjusts to new conformations to form a new coordination sphere due to the small displacement of the Thr14 (Table 1). As with the p15Y/CDK5/p25/ATP/HHASPRK complex and the previous crystal structural investigation, oxygen atoms of Asn131 and Asn144 can also offer coordination interactions correctly except for the 3 coordinations from ATP. Since the water molecule gives rise to a strong and stable coordination, Mg^{2+} has an accurate hexacoordination sphere in the CDK5/p25/ATP/HHASPRK system. This is crucial for the phosphate group transfer. The importance of the water molecule will be discussed later.

Energetic Properties of All the Complexes. The negative electrostatic (ELE_{tot}) values in the binding energies of all the complexes indicate that the electrostatic interactions are favorable in the association between ATP and the receptors, and the gas phase electrostatic contributions (ELE_g) are more dominant. Observing the $E_{vdw} + \Delta G_{nonpolar}$ contributions, it is clear the van der Waals/nonpolar interactions also facilitate the binding of the substrate to the kinase, although the interactions are relatively weaker. The smaller ELE_s value of the pT14 complex is possibly caused by the displacement of the ATP phosphate group. The displaced group is closer to the edge of the active site, comparing with that in the other two complexes, which means that less desolvation energy is needed during the process of ATP entering into the active site. As a result, the ELE_{tot} of the pT14 system is lower than that of the unphosphorylated complex although the gas phase electrostatic contribution in the pT14 complex (−1232.84 kcal/mol) is obviously weaker than those of the pY15 and the unphosphorylated systems, which are −1394.69 and −1352.98 kcal/mol, respectively, due to the compensation of the ELE_s contributions.

Considering the structural similarities and differences in the binding of ATP in the CDK5/p25/ATP/HHASPRK and the p15Y/CDK5/p25/ATP/HHASPRK combinations, analyses of binding energy and energy decomposition were also carried out to illustrate the mechanism of CDK activation by phosphorylation on the Tyr15. Hydrogen-bonding interactions between ATP and the protein in all the systems are compared by combining a gas phase electrostatic contribution analysis. As presented in Table 2, the number of HBs between ATP and kinase with duration longer than 50% in the p15Y/CDK5/p25/ATP/HHASPRK, CDK5/p25/ATP/HHASPRK, and p14T/CDK5/p25/ATP/HHASPRK combinations are 5, 5, and 4, respectively, with averaged bond lengths of 2.86 Å, 2.85 Å, and 2.95 Å. This means that, after ATP entered into the active site, there are more and stronger electrostatic interactions in the former two complexes than in the third. As reflected by the values given in Table 3, the ELE_g contributions in the p15Y, unphosphorylated, and the

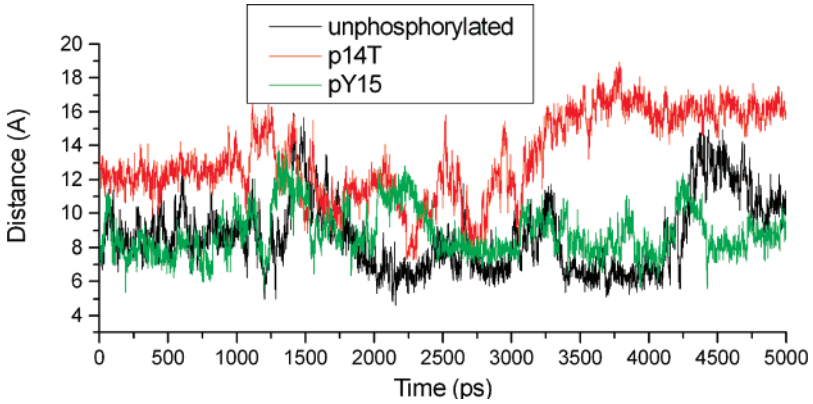

FIGURE 5: Swinging motion of R side chain in all complexes.

p14T systems are −1394.69 kcal/mol, −1352.98 kcal/mol, and −1232.84 kcal/mol, respectively. This suggests that the misalignment of the phosphate group in the ATP-binding cleft severely impairs the hydrogen-bonding environment in the complex.

The coordination sphere and the contributions from groups around the ion are explored to illustrate the importance of the correct coordinating environment from an energy point of view. As discussed above, the ion shares different coordination environments in these three complexes. In the p14T system, it is pentacoordinated (Figure 2c); in the p15Y complex (Figure 2a), a hexacoordination exists; and in the unphosphorylated combination, it is also hexacoordinated (Figure 2b) but occurs with different coordination contributors in comparison with that in the p15Y complex. By calculating the binding energies between the ion and the rest of the complexes when the water molecule is included or excluded, it is clear that about −80 kcal/mol energy contribution is from the water molecule, which makes it an important coordination factor. Hence, a missing coordinated water molecule in the coordination environment might cause very serious consequences to the transfer reaction.

Taking into account the strong chelation between the oxygen atoms on the phosphate group, it is not surprising why the misalignment of the phosphate group can also pull the Mg^{2+} along with its displacement and so cause an obvious shift of the ion in the pT14 complex.

Binding of Substrate Peptide. According to Bártová et al. (*35*, *36*), the insertion of the negatively charged phosphate group at the Thr14 or the Tyr15 position causes the positively charged R side chain in the CDK2 systems to interact with this group. However, different behaviors of the side chain are detected in our simulations. As seen in Figure 5, the shape of the distance curve describing the side chain movement is similar to the peptide RMSD curves, suggesting that the RMSD oscillation mainly results in the movement of the R side chain, even though the reason of the swinging remains unclear.

Due to the structural differences between cyclinA and p25, some clashes exist between the terminal K side chain and the α3-α4 loop when the initial structures were generated. Consequently, the K side chain has to adjust its conformation or position to eliminate the clashes to keep the peptide in the substrate binding box during the simulations. The side chain can stretch either toward the cleft sandwiched by the CDK5 and p25 or toward the outside of the cleft. Our simulations, however, give both possibilities; in the p14T complex, the side chain points into the cleft, and in the other two combinations, it extends to the outside of the cleft. By looking into the binding energy contribution from three crucial residues (Asn387, Glu388, and Ile389) on p25 interacting with the lysine, it is found that the residues contribute similarly to the binding even if they interact with the different conformations of the lysine side chain. In the p15Y, p14T, and unphosphorylated systems, the contributions from the 3 residues are −140.19 kcal/mol, −126.34 kcal/mol, and −133.74 kcal/mol, respectively, indicating that the conformation of the residue has minor influence on the peptide binding with the p25 part.

REFERENCES

1. Harper, J. W., and Adams, P. D. (2001) Cyclin-dependent kinases, *Chem. Rev. 101*, 2511−2526.
2. Garrett, M. D., and Fattaey, A. (1999) CDK inhibition and cancer therapy, *Curr. Opin. Genet. Dev. 9*, 104−111.
3. Webster, K. R. (1998) The therapeutic potential of targeting the cell cycle, *Expert. Opin. Invest. Drugs 7*, 865−887.
4. Dhavan, R., and Tsai, L. H. (2001) A decade of Cdk5, *Nat. Rev. Mol. Cell Biol. 2*, 749−759.
5. Tarricone, C., Dhavan, R., Peng, J., Areces, L. B., Tsai, L-H., and Musacchio, A. (2001) A: Structure and regulation of the CDK5-p25 (nck5a) complex, *Mol. Cell 8*, 657−669.
6. Nguyen, M. D., and Julien, J. P. (2003) Cyclin-dependent kinase 5 in amyotrophic lateral sclerosis, *Neurosignals 12*, 215−220.
7. Lau, L. F., and Ahlijanian, M. K. (2003) Role of cdk5 in the pathogenesis of Alzheimer's disease, *Neurosignals 12*, 209−214.
8. Smith, P. D., Crocker, S. J., Jackson-Lewis, V., Jordan-Sciutto, K. L., and Hayley, S. (2003) Cyclin-dependent kinase 5 is a mediator of dopaminergic neuron loss in a mouse model of Parkinson's disease, *Proc. Natl. Acad. Sci. U.S.A. 100*, 13650−13655.
9. Bu, B., Li, J., Davies, P., and Vincent, I., J. (2002) Deregulation of cdk5, hyperphosphorylation, and cytoskeletal pathology in the Niemann-Pick type C murine model, *J. Neurosci. 22*, 6515−6125.
10. Wang, J., Liu, S., Fu, Y., Wang, J. H., and Lu, Y. (2003) Cdk5 activation induces CA1 pyramidal cell death by direct phosphorylating NMDA receptors, *Nat. Neurosci. 6*, 1039−1047.
11. Hunter, T., and Pines, J. (1994) Cyclins and CancerII: Cyclin D and CDK Inhibitors Come of Age, *Cell 79*, 573−582.
12. Sherr, C. (1996) Cancer cell cycles, *Science 274*, 1672−1677.
13. Norbury, C., and Nurse, P. (1992) Animal Cell Cycles and Their Control, *Annu. Rev. Biochem. 61*, 441−470.
14. De Azevedo, W. F., Jr., Mueller-Dieckmann, H. J., Schulze-Gahmen, U., Worland, P. J., Sausville, E., and Kim, S. H. (1996) Structural basis for specificity and potency of a flavonoid inhibitor of human CDK2, a cell cycle kinase, *Proc. Natl. Acad. Sci. U.S.A. 93*, 2735−2740.
15. De Azevedo, W. F., Jr., Leclerc, S., Meijer, L., Havlicek, L., Strnad, M., and Kim, S. H. (1997) Inhibition of cyclin-dependent

kinases by purine analogues: crystal structure of human cdk2 complexed with roscovitine, *Eur. J. Biochem. 243*, 518−526.
16. Baumann, K., Mandelkow, E. M., Biernat, J., Piwnica-Worms, H., and Mandelkow, E. (1993) Abnormal Alzheimer-like phosphorylation of tau protein by cyclin-dependent kinases cdk2 and cdk5, *FEBS Lett. 336*, 417−424.
17. Fletcher, A. I., Shuang, R., Giovannucci, D. R., Zhang, L., Bittner, M. A., and Stuenkel, E. L. (1999) Regulation of Exocytosis by Cyclin-dependent Kinase 5 via Phosphorylation of Munc18, *J. Biol. Chem. 274*, 4027−4035.
18. Hisanaga, S., Ishiguro, K., Uchida, T., Okumura, E., Okano, T., and Kishimoto, T. (1993) Tau protein kinase II has a similar characteristic to cdc2 kinase for phosphorylating neurofilament proteins, *J. Biol. Chem. 268*, 15056−15060.
19. Ishiguro, K., Takamatsu, M., Tomizawa, K., Omori, A., Takahashi, M., Arioka, M., Uchida, T., and Imahori, K. (1992) Tau Protein Kinase I Converts Normal Tau Protein into A68-like Component of Paired Helical Filaments, *J. Biol. Chem. 267*, 10897−10901.
20. Lew, J., Winkfein, R. J., Paudel, H. K., and Wang, J. H. (1992) Brain proline-directed protein kinase is a neurofilament kinase which displays high sequence homology to p34cdc2, *J. Biol. Chem. 267*, 25922−25926.
21. Matsubara, M., Kusubata, M., Ishiguro, K., Uchida, T., Titani, K., and Taniguchi, H. (1996) Site-specific Phosphorylation of Synapsin I by Mitogen-activated Protein Kinase and Cdk5 and Its Effects on Physiological Functions, *J. Biol. Chem. 271*, 21108−21113.
22. Niethammer, M., Smith, D. S., Ayala, R., Peng, J., Ko, J., Lee, M. S., Morabito, M., and Tsai, L. H. (2000) NUDEL is a novel Cdk5 substrate that associates with LIS1 and cytoplasmic dynein, *Neuron 28*, 697−711.
23. Paudel, H. K., Lew, J., Ali, Z., and Wang, J. H. (1993) Brain proline-directed protein kinase phosphorylates tau on sites that are abnormally phosphorylated in tau associated with Alzheimer's paired helical filaments, *J. Biol. Chem. 268*, 23512−23518.
24. Shuang, R., Zhang, L., Fletcher, A., Groblewski, G. E., Pevsner, J., and Stuenkel, E. L. (1998) Regulation of Munc-18/Syntaxin 1A Interaction by Cyclin-dependent Kinase 5 in Nerve Endings, *J. Biol. Chem. 273*, 4957−4966.
25. Johnson, L. N., and Lewis, R. J. (2001) Structural basis for control by phosphorylation, *Chem. Rev. 101*, 2209−2242.
26. Beaudette, K., Lew, J., and Wang, J. H. (1993) Substrate specificity characterization of a cdc2-like protein kinase purified from bovine brain, *J. Biol. Chem. 268*, 20825−20830.
27. Songyang, Z., Lu, K. P., Kwon, Y. T., Tsai, L. H., Filhol, O., Cochet, C., Brickey, D. A., Soderling, T. R., Bartleson, C., Graves, D. J., DeMaggio, A. J., Hoekstra, M. F., Blenis, J., Hunter, T., and Cantley, L. C. (1996) A structural basis for substrate specificities of protein Ser/Thr kinases: primary sequence preference of casein kinases I and II, NIMA, phosphorylase kinase, calmodulin-dependent kinase II, CDK5, and Erk1, *Mol. Cell. Biol. 16*, 6486−6493.
28. Moreo, S., and Nurse, P. (1990) Substrates for p34cdc2: in vivo veritas?, *Cell 61*, 549−551.
29. Jeffrey, P. D., Russo, A. A., Polyak, K., Gibbs, E., Hurwitz, J., Massague, J., and Pavletich, N. P. (1995) Mechanism of CDK activation revealed by the structure of a cyclinA-CDK2 complex, *Nature 376*, 313−320.
30. Russo, A., Jeffrey, P. D., and Pavletich, N. P. (1996) Structural basis of cyclin-dependent kinase activation by phosphorylation, *Nat. Struct. Biol. 3*, 696−700.
31. Gu, Y., Rosenblatt, J., and Morgan, D. O. (1992) Cell cycle regulation of CDK2 activity by phosphorylation of Thr160 and Tyr15, *EMBO J. 11*, 3995−4005.
32. Poon, R. Y., Lew, J., and Hunter, T. (1997) Identification of Functional Domains in the Neuronal Cdk5 Activator Protein, *J. Biol. Chem. 272*, 5703−5708.
33. Zukerberg, L. R., Patrick, G. N., Nikolic, M., Humbert, S., Wu, C. L., Lanier, L. M., Gertler, F. B., Vidal, M., Van Etten, R. A., and Tsai, L. H. (2000) Cables links Cdk5 and c-Abl and facilitates Cdk5 tyrosine phosphorylation, kinase upregulation, and neurite outgrowth, *Neuron 26*, 633−646.
34. Cook, A., Lowe, E. D., Chrysina, E. D., Skamnaki, V. T., Oikonomakos, N. G., and Johnson, L. N. (2002) Structural studies on phospho-CDK2/cyclin A bound to nitrate, a transition state analogue: implications for the protein kinase mechanism, *Biochemistry 41*, 7301−7311.
35. Bártová, I., Otyepka, M., Kříž, Z., and Koča, J. (2004) Activation and inhibition of cyclin-dependent kinase-2 by phosphorylation; a molecular dynamics study reveals the functional importance of the glycine-rich loop, *Protein Sci. 13*, 1449−1457.
36. Bártová, I., Otyepka, M., Kříž, Z., and Koča, J. (2005) The mechanism of inhibition of the cyclin-dependent kinase-2 as revealed by the molecular dynamics study on the complex CDK2 with the peptide substrate HHASPRK, *Protein Sci. 14*, 445−451.
37. Welburn, J. P. I., Tucker, J. A., Johnson, T., Lindert, L., Morgan, M., Willis, A., Noble, M. E. M., and Endicott, J. A. (2007) How Tyrosine 15 Phosphorylation Inhibits the Activity of Cyclin-dependent Kinase 2-Cyclin A, *J. Biol. Chem. 282*, 3173−3181.
38. Brown, N. R., Noble, M. E. M., Endicott, J. A., and Johnson, L. N. (1999) The structural basis for specificity of substrate and recruitment peptides for cyclin-dependent kinases, *Nat. Cell Biol. 1*, 438−443.
39. Cornell, W. D., Cieplak, P., Bayly, C. I., Gould, I. R., Merz, K. M., Ferguson, D. M., Jr., Spellmeyer, D. C., Fox, T., Caldwell, J. W., and Kollman, P. A. (1995) A Second Generation Force Field for the Simulation of Proteins, Nucleic Acids, and Organic Molecules, *J. Am. Chem. Soc. 117*, 5179−5197.
40. Besler, B. H., Merz, K. M., and Kollman, P. A. (1990) Atomic Charges Derived from Semiempirical Methods, *J. Comput. Chem. 11*, 431−439.
41. Fox, T., and Kollman, P. A. (1998) Application of the RESP methodology in the Parametrization of Organic Solvents, *J. Phys. Chem. B 102*, 8070−8079.
42. Case, D. A., Pearlman, D. A., Caldwell, J. W., Cheatham III, T. E., Wang, J., Ross, W. S., Simmerling, C. L., Darden, T. A., Merz, K. M., Stanton, R. V., Cheng, A. L., Vincent, J. J., Crowley, M., Tsui, V., Gohlke, H., Radme, R. J., Duan, Y., Pitera, J., Massova, I., Seibel, G. L., Singh, U. C., Weiner, P. K., and Kollman, P. A. (2004) *AMBER 8*, University of California, San Francisco.
43. Jorgensen, W. L., Chandrasekhar, J., Madura, J. D., Impey, R. W., and Klein, M. L. (1983) Comparison of simple potential functions for simulating liquid water, *J. Chem. Phys. 79*, 926−935.
44. Darden, T., York, D., and Pedersen, L. (1993) An. N.log(N) method for Ewald sums in large systems, *J. Chem. Phys. 98*, 10089−10092.
45. Ryckaert, J. P., Ciccotti, G., and Berendsen, H. J. C. (1997) Numerical integration of the Cartesian equations of motion of a system with constraints: Molecular dynamics of n-alkanes, *J. Comput. Phys. 23*, 327−341.
46. Berendsen, H. C., Postma, J. P. M., van Gunsteren, W. F., DiNola, A., and Haak, J. R. (1984) Molecular-dynamics with coupling to an external bath, *J. Chem. Phys. 81*, 3684−3690.
47. Massova, I., and Kollman, P. A. (2000) Combined molecular mechanical and continuum solvent approach (MM-PBSA/GBSA) to predict ligand binding, *Perspect. Drug Discovery 18*, 113−135.
48. Zhang, B., Tan, V. B. C., Lim, K. M., and Tay, T. E. (2006) Molecular dynamics simulations on the inhibition of Cyclin-Dependent Kinase 2 and 5 in the presence of activators, *J. Comput.-Aided Mol. Des. 20*, 395−404.
49. Zhang, B., Tan, V. B. C., Lim, K. M., and Tay, T. E. (2007) Study of the inhibition of cyclin-dependent kinases with roscovitine and indirubin-3′-oxime from molecular dynamics simulations, *J. Mol. Model. 13*, 79−89.
50. Zhuang, S. L., Zou, J. W., Jiang, Y. J., Mao, X., Zhang, B., Liu, H. C., and Yu, Q. S. (2005) Some Insights into the Stereochemistry of Inhibition of Macrophage Migration Inhibitory Factor with 2-Fluoro-*p*-hydroxycinnamate and Its Analogues from Molecular Dynamics Simulations *J. Med. Chem. 48*, 7208−7214.
51. Bao, J., Zhang, D. W., Zhang, J. Z. H., Lee Huang, P., Lin Huang, P., and Lee-Huang, S. (2007) Computational study of bindings of olive leaf extract (OLE) to HIV-1 fusion protein gp41, *FEBS Lett. 581*, 2737−2742.
52. Hou, T. J., Guo, S. L., and Xu, X. J. (2002) Predictions of Binding of a Diverse Set of Ligands to Gelatinase-A by a Combination of Molecular Dynamics and Continuum Solvent Models, *J. Phys. Chem. B 106*, 5527−5535.
53. Sanner, M. F., Olson, A. J., and Spehner, J.-C. (1996) Reduced surface: an efficient way to compute molecular surfaces. *Biopolymers 38*, 305−320.
54. Sitkoff, D., Sharp, K. A., and Honig, B. (1994) Accurate calculation of hydration free energies using macroscopic solvent models, *J. Phys. Chem. 98*, 1978−1988.
55. Wang, J. M., Morin, P., Wang, W., and Kollman, P. A. (2001) Use of MM-PBSA in reproducing the binding free energies to

HIV-1 RT of TIBO derivatives and predicting the binding mode to HIV-1 RT of efavirenz by docking and MM-PBSA, *J. Am. Chem. Soc. 123*, 5221−5230.
56. Hemmer, W., McGlone, M., Tsigelny, I., and Taylor, S. S. (1997) Role of the Glycine Triad in the ATP-binding Site of cAMP-dependent Protein Kinase, *J. Biol. Chem. 272*, 16946−16954.
57. Tsigelny, I., Greenberg, J. P., Cox, S., Nichols, W. L., Taylor, S. S., and Ten Eyck, L. F. (1999) 600 ps molecular dynamics reveals stable substructures and flexible hinge points in cAMP dependent protein kinase, *Biopolymers 50*, 513−524.
58. Aimes, R. T., Hemmer, W., and Taylor, S. S. (2000) Serine-53 at the Tip of the Glycine-Rich Loop of cAMP-Dependent Protein Kinase: Role in Catalysis, P-Site Specificity, and Interaction with Inhibitors, *Biochemistry 39*, 8325−8332.

BI700890T